

Visible Light Communication based Vehicle Localization and Pose Estimation

Burak Soner, *Student Member, IEEE*, and Sinem Coleri, *Senior Member, IEEE*,

Abstract—Autonomous vehicles need to estimate the relative poses, i.e., position and orientation, of the surrounding vehicles on the road with at least 50 Hz rate and cm-level accuracy for platooning and collision avoidance applications. The LIDAR/camera solutions currently used for vehicle pose estimation do not satisfy these rate and accuracy requirements, necessitating complementary technologies. Vehicular visible light positioning (VLP) is a highly suitable complementary technology due to its high rate and high accuracy, exploiting the line-of-sight propagation feature of the visible light communication (VLC) signals from LED head/tail lights. However, existing vehicular VLP solutions impose restrictive requirements, e.g., high-bandwidth circuit, base station and VLC waveform constraints, and work for limited relative vehicle orientations, thus, cannot be extended for pose estimation. This paper proposes a VLP-based vehicle pose estimation (VLP-VPE) solution that eliminates these restrictive requirements by a novel VLC receiver design and a novel pose estimation algorithm. The VLC receiver, named QRX, is low-cost/size, and enables high-rate VLC and high-accuracy angle-of-arrival sensing, simultaneously, via the usage of a quadrant photodiode. The estimation algorithm first uses two of the designed QRXs to determine the positions of two head/tail light VLC transmitters on a neighbouring vehicle via triangulation, and then determines the 2D pose of the vehicle based on these two positions. Sensitivity analyses and simulations using traffic data from the Simulation of Urban Mobility (SUMO) demonstrate that the proposed solution performs pose estimation at cm-level accuracy and kHz rate under realistic road and channel conditions, demonstrating its eligibility for platooning and collision avoidance applications.

Index Terms—autonomous vehicles, platooning, collision avoidance, pose estimation, visible light communication.

I. INTRODUCTION

AUTOMOTIVE research is currently heavily oriented towards vehicular automation and autonomy, and the foremost objective is improving driving safety and efficiency [1]. The annual traffic accident report published by the Federal Statistical Office of Germany (Destatis) [2] shows that 63% of traffic accidents are vehicle-to-vehicle collisions, demonstrating the importance of collision avoidance systems and safe platooning for future automated/autonomous vehicle safety concepts [3]. Collision avoidance and platooning systems need to estimate the poses of surrounding vehicles at >50 Hz rate and cm-level accuracy with high reliability and availability under harsh road conditions [4–6].

Current sensor solutions, which are readily being used for less demanding conventional autonomous driving tasks,

Burak Soner and Sinem Coleri are with the Department of Electrical and Electronics Engineering, Koc University, 34450 Istanbul, Turkey (e-mail: bsoner16@ku.edu.tr, scoleri@ku.edu.tr). Burak Soner is also with Koc University Ford Otosan Automotive Technologies Laboratory (KUFOTAL), Istanbul, Turkey. The authors acknowledge the support of Ford Otosan and the Scientific and Technological Research Council of Turkey EU CHIST-ERA grant # 119E350.

fail to meet the rate and accuracy requirements of collision avoidance and platooning systems [6]. Differential Global Positioning System (DGPS), which is used for global self-localization, allows vehicles to also cooperatively localize each other. However, this sensor provides only meter-level accuracy at ≤ 20 Hz rate [7], and, does not provide pose estimation since it regards vehicles as point objects. Alternatively, LIDAR [8] and camera-based methods [9], which are used for the localization of non-vehicle objects on the road, can be used for estimating vehicle pose at up to cm-level accuracy. However, the estimation rate of these solutions is limited to ≤ 50 Hz since they typically require scanning, locating and labelling millions of points/pixels for estimating vehicle pose [10, 11]. On the other hand, communication-based positioning methods, which promise estimation of vehicle antenna locations at cm-level accuracy and kHz rate, can be extended for pose estimation, enabling collision avoidance and safe platooning applications and complementing the existing autonomous driving system for higher safety.

Communication-based positioning algorithms in the vehicular domain mainly employ radio frequency (RF) technologies such as cellular and dedicated short range communications (DSRC) [12], and VLC technologies [13–15]. Cellular-based positioning works either utilize location-fingerprinted received signal strength (RSS) measurements or apply triangulation via signal parameters such as time-of-arrival (ToA), time-difference-of-arrival (TDoA) and angle-of-arrival (AoA) [16]. However, these methods rely on tight synchronization between base stations and the mobile terminal, with their accuracy limited due to excessive multipath interference. Although pilot-based synchronization methods [17] and estimators like multiple signal classification (MUSIC) [18] somewhat mitigate these problems, overall cellular-based positioning accuracy is >10 m in practical scenarios [19, 20]. DSRC suffers from similar issues; while roundtrip-time-of-flight (RToF) methods successfully mitigate synchronization issues [21, 22], the best reported accuracy is $\approx 1\text{--}10$ m [23], still not meeting the cm-level requirement. As an alternative, vehicular VLP methods based on line-of-sight (LoS) VLC signals from automotive LED head and tail lights fundamentally promise cm-level accuracy at $\gg 50$ Hz rates [14, 24]. However, this promise is not fulfilled in practice since existing vehicular VLP methods impose restrictive requirements such as high-bandwidth circuit, base station and VLC waveform constraints, and they only work for limited relative vehicle orientations.

Previous works in vehicular VLP use TDoA [25], phase-difference-of-arrival (PDoA) [14, 26], RToF [27, 28] and AoA [29–31] approaches. In [25], the TDoA of a VLC signal from localized traffic lights to two on-board photodiodes

is utilized for finding the relative position of a vehicle. This method provides only ≈ 1 m accuracy and has very low availability since it restrictively requires the presence of localized traffic lights. In [14] and [26], the PDoA of head/tail light VLC signals to two photodiodes on a vehicle provides cm-level positioning. However, the method restrictively assumes that the vehicles are oriented parallel to each other and requires very high frequency constant tones (10-50MHz), which cannot practically be transmitted to useful distances with automotive LEDs [32]. Recently, [27] and [28] have achieved cm-level longitudinal range estimation at kHz rate based on the RTToF of a VLC message between two vehicles. However, this method requires special high-bandwidth circuits and restrictively assumes longitudinally parallel vehicles, hence, cannot translate VLP to full pose estimation. A vehicular VLP method that eliminates these restrictive requirements with further extension into pose estimation is necessary for collision avoidance and platooning applications.

AoA-based VLP methods promise high accuracy without imposing restrictive requirements such as limited vehicle orientations, and base station, high-bandwidth circuit and VLC waveform constraints [29]. However, their vehicular implementations have so far been limited to camera-VLC based methods. Camera-VLC approaches are not suitable since they either provide very low (<kbps [32]) communication rates [30] or require costly high-frame-rate cameras [31], which beats the purpose of VLP complementing sensor solutions. Therefore, a low-cost and small-size photodiode-based VLC receiver (RX) design that can provide high-rate VLC and high-accuracy, high-resolution and high-rate AoA measurement, is needed.

Existing photodiode-based VLC RX designs that can be used for AoA measurement fall into four main categories [33]: aperture-based, lens-based, prism-based and tilted-photodiode-based designs. Tilted-photodiode designs [34–37] and special prism-based designs [38] are not suitable for vehicular use since they are not low-cost/size and typically provide limited AoA resolution. Aperture-based designs using commercially available low-cost/size quadrant-photodiodes (originally proposed for angular diversity in multiple-input-multiple-output (MIMO) indoor VLC [39–41]) can be used for accurate and resolute AoA measurement but the aperture limits the field-of-view (FoV). Using an imaging architecture, e.g., a hemispherical lens rather than an aperture, provides larger FoV [42]. Such quadrant-photodiode-based imaging designs, traditionally used for laser target tracking [43] and transceiver pointing [44], are also promising for AoA measurement. A low-cost/size realization of this architecture with commercial off-the-shelf (COTS) components would enable the restriction-free AoA-based high accuracy and rate vehicular VLP method.

In this paper, we propose a VLP-based vehicle pose estimation (VLP-VPE) solution that uses only two on-board AoA-sensing receivers for obtaining the relative 2D pose of a transmitting vehicle. First, we provide a novel low-cost/size quadrant-photodiode-based AoA-sensing VLC RX (QRX) design. This design enables the first practical vehicular implementation of an AoA-based VLP method with cm-level accuracy at kHz rate. We then extend VLP into vehicle pose estimation. Two QRX units located at the head/tail lights

measure the AoA from two VLC head/tail light transmitters (TX) on the target vehicle and locate the position of each TX separately via triangulation (i.e., two AoAs and the inter-QRX distance defines a triangle). The two TX unit positions, which are known locations on the frame of the target vehicle, are then used to determine its pose, i.e., its position and orientation. This work extends our previous related work, where a single AoA-sensing RX model is considered for VLP but the RX design is not presented and the VLP method necessitates the target vehicle to disseminate its heading and speed information via VLC [45]. This paper provides design details for the QRX, and the solution proposed in this paper, which further extends VLP into pose estimation, does not require any such co-operation from the transmitting vehicle since it applies triangulation directly with two on-board QRXs. The main contributions of this paper are given as follows:

- We present a novel low-cost/size QRX design, which uses only COTS components and enables high-rate VLC and high-accuracy, high-resolution and high-rate AoA measurement, simultaneously, for the first time in the literature. The design is a quadrant-photodiode-based imaging receiver similar to [42] but specifically designed for AoA-based vehicular VLP.
- We propose an AoA-based vehicular VLP method that uses the designed QRX and promises cm-level accuracy and kHz rate positioning without imposing any restrictive requirements like base station, high-bandwidth circuit and waveform constraints, for the first time in the literature.
- We extend the proposed VLP method into a vehicle pose estimation solution, which meets the cm-level accuracy and >50 Hz rate requirements of collision avoidance and platooning applications, for the first time in the literature.
- We perform an extensive performance evaluation for the proposed vehicle pose estimation solution. First, we determine the theoretical bound for pose estimation accuracy with respect to VLC channel noise via differential sensitivity analysis. Then, through extensive simulations, we demonstrate that cm-level pose estimation accuracy is achieved at kHz rate under realistic road and channel conditions, demonstrating the eligibility of the proposed solution for use in collision avoidance and platooning applications.

The rest of the paper is organized as follows. Section II presents the system model and the problem description for vehicle pose estimation. Section III provides the novel low-cost/size QRX design. Section IV presents the proposed VLP-VPE solution that uses the designed QRX, and the theoretical analysis of its performance via differential sensitivity analysis. Section V demonstrates the performance of the proposed solution at the required accuracy and rate for collision avoidance and platooning via simulations in a custom MATLAB®-based vehicular VLC simulator coupled with the Simulation of Urban Mobility (SUMO) package [46] under realistic road and VLC channel conditions. Section VI concludes the paper.

II. SYSTEM MODEL AND PROBLEM DEFINITION

This section first presents the VLC/VLP-capable vehicle model considered in this work and then defines the vehicle pose estimation problem in collision avoidance and platooning.

A. System Model

The model considers the following assumptions (A#):

- A1: Vehicles drive on piecewise-flat roads, i.e., neighbouring vehicles share flat road sections and have no pitch angle difference between them. This assumption, which allows to define the pose estimation problem in 2D, is reasonably valid for collision avoidance and platooning scenarios since these scenarios consider vehicles within ≤ 20 m of each other driving at ≥ 30 km/h [3, 47, 48].
- A2: Vehicles contain two VLC units each on both front and rear faces, i.e., on LED head/tail lights. Each VLC unit utilizes its LEDs as the TX, contains one AoA-sensing receiver (QRX), and sustains reliable LoS VLC with other units in its FoV.
- A3: Transmissions by the VLC units do not interfere. This can be achieved through the design of a medium access control mechanism for the network containing VLC units, on both the same vehicle and neighbouring vehicles, such that no two units transmit at the same time on the same frequency band when their lines-of-sight are towards the same receiver [49, 50].
- A4: QRXs are well-calibrated and free of systematic errors. Therefore, the major factor affecting their AoA estimation accuracy is the additive white gaussian noise (AWGN) on the VLC channel.

The system model is visualized in Fig. 1. The red vehicle implements AoA-based VLP with two on-board QRX units to find the relative positions of both rear TX units on the green vehicle. These two positions sufficiently define its relative pose, i.e., its position and orientation. A vehicle is termed “ego” (red in Fig. 1) if it is computing the relative pose of a nearby vehicle and “target” (green in Fig. 1) if its relative pose is being computed by a nearby ego vehicle. In this paper, TX units are in the target vehicle and RX units are in the ego vehicle, but a vehicle can take on either role since it contains both TX and RX units in both head and tail lights.

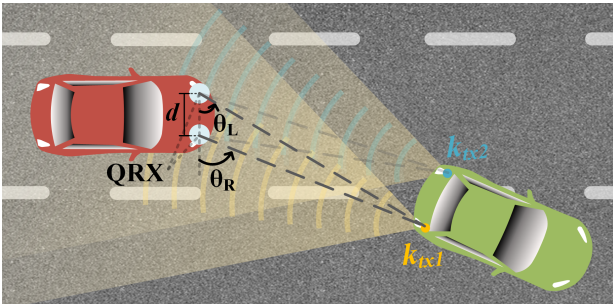


Fig. 1. System model. θ_R, θ_L : AoA at the right and left QRX, respectively. d : QRX separation. k_{tx1}, k_{tx2} : positions of TX1 and TX2, respectively.

B. Problem Definition

The pose estimation problem in collision avoidance and platooning considers estimating the position and orientation of the target vehicle relative to the ego vehicle. In mathematical terms, this corresponds to estimating the translation and rotation of the target vehicle frame with respect to the ego vehicle frame, as shown in Fig. 2a. Translation is defined as the x and y displacement of the target frame origin, i.e., O_t , from the ego frame origin, i.e., O_e , and is represented by ${}^e x_t$ and ${}^e y_t$ for x and y, respectively. Rotation is defined as the difference between the orientations of the two frames, i.e., the angle between the respective axes of the two frames when translation between them is zero, and is represented by φ .

Conventional solutions estimate $({}^e x_t, {}^e y_t)$ and φ , thus, vehicle pose, via LIDAR/cameras. However, these solutions are not robust and incur a significant computational load; since LIDAR/cameras cannot identify the points they locate, i.e., provide “unlabelled” points, they necessitate additional correlation-based techniques to first identify, i.e., “label”, the points belonging to vehicle features, which are then used for estimating pose [8]. Alternatively, using two beacon-like features provides a much simpler approach; two such positions on the vehicle, which are “labelled” *per se*, are sufficient for determining $({}^e x_t, {}^e y_t)$ and φ , thus, vehicle pose, by

$$\varphi = \arctan \left(\frac{|{}^e x_{tx1} - {}^e x_{tx2}|}{|{}^e y_{tx1} - {}^e y_{tx2}|} \right) \quad (1)$$

$$\begin{bmatrix} {}^e x_t \\ {}^e y_t \end{bmatrix} = \begin{bmatrix} {}^t x_{tx2} \\ {}^t y_{tx2} \end{bmatrix} - \begin{bmatrix} \cos(\varphi) & \sin(\varphi) \\ -\sin(\varphi) & \cos(\varphi) \end{bmatrix} \begin{bmatrix} {}^e x_{tx2} \\ {}^e y_{tx2} \end{bmatrix}, \quad (2)$$

where $({}^e x_{tx1}, {}^e y_{tx1})$ and $({}^e x_{tx2}, {}^e y_{tx2})$ denote x/y displacements of the two labelled target vehicle beacons, i.e., TX1 and TX2, respectively, from O_e , and $({}^t x_{tx2}, {}^t y_{tx2})$ denotes x/y displacement of TX2 from O_t , as shown in Fig. 2b. TX1 could equivalently be used in Eqn. (2). Therefore, two TX unit positions, which can be located by triangulation-based VLP utilizing AoA measurements from the novel QRX, sufficiently define the vehicle pose.

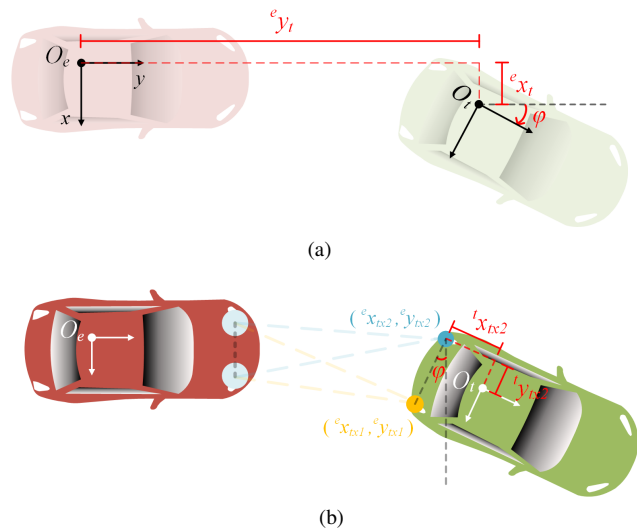


Fig. 2. (a) Vehicle pose is defined by translation and rotation of the target frame with respect to the ego frame. (b) Triangulation-based VLP methods locating two head/tail light TXs can be used for pose estimation.

III. AOA-SENSING VEHICULAR VLC RECEIVER

This section presents the novel AoA-sensing VLC RX design, i.e., QRX, which promises high-rate communication and high-accuracy, high-resolution and high-rate AoA measurement, simultaneously. This design is also low-cost since it uses COTS components only, enabling the practical realization of the VLP-VPE solution.

A conceptual diagram of the QRX and its optical configuration are shown in Fig. 3 and a prototype of the QRX built with low-cost COTS components is shown in Fig. 4. The design of the QRX is inspired by the MIMO VLC RX in [42] but the QRX is specifically designed for high-resolution AoA measurement in VLP rather than simply achieving angular diversity. The QRX contains a hemispherical lens placed at a certain distance above a quadrant-photodiode (QPD), focusing the rays from the TX LED into a spot. The position of the spot on the QPD, which depends on AoA by ray optics relations, determines the received signal power on each quadrant as depicted in Fig. 3. Let f_{QRX} be the function that relates the AoA, θ , to the signal power ratio between horizontally separated quadrants, Φ_h , by

$$\Phi_h = f_{QRX}(\theta) = \frac{(\epsilon_B + \epsilon_D) - (\epsilon_A + \epsilon_C)}{\epsilon_A + \epsilon_B + \epsilon_C + \epsilon_D}, \quad (3)$$

where ϵ_i represents the power of the received signal in quadrant i , $i \in \{A, B, C, D\}$, and Φ_h is bound to the $[-1, 1]$ interval and can be calculated from quadrant received signal power readings online. Choosing an f_{QRX} function is the main task in QRX design since the inverse of f_{QRX} , which we call g_{QRX} , is used in the estimation of θ (AoA); g_{QRX} is computed to sufficient precision by ray optics simulations offline (A4) and is stored in the form of a 1D look-up table on the ego vehicle.

f_{QRX} is determined by the optical configuration parameters, i.e., lens diameter, lens refractive index, QPD size and lens-QPD distance, denoted by d_L , n , d_H , d_X , respectively, as also shown in Fig. 3. d_L , n and d_X determine the spot diameter, i.e., $2d_R$, where d_R is the spot radius [51]:

$$2d_R = \frac{(d_L)(d_L/n - d_X)}{d_L/n} = d_L - (n)(d_X). \quad (4)$$

The relative size of $2d_R$ and d_H determines the conformance of f_{QRX} to its design goals, which are: high FoV (ideally $\pm 90^\circ$), high linearity, and bijection, i.e., being one-to-one and onto. For given d_H , larger $2d_R$ provides higher FoV but worse linearity [43]. Furthermore, $2d_R > d_H\sqrt{2}$ violates bijection since in such configurations, all quadrants remain completely within the effective spot area and receive equal signal power for spot positions around the center [52], i.e., θ values around zero become undetectable since they all result in $\Phi_h = 0$, as in the blue curve in Fig. 5. Therefore, recognizing these trade-offs, 1) a lens-QPD pair, i.e., $\{d_L, n, d_H\}$, and 2) the lens-QPD distance, i.e., d_X , should be chosen to obtain the best compromise for the three design goals.

1) *Choosing a lens-QPD pair:* The primary objective while choosing a lens-QPD pair is ensuring bijection. First, a low-cost and high-bandwidth COTS QPD is chosen to set d_H .

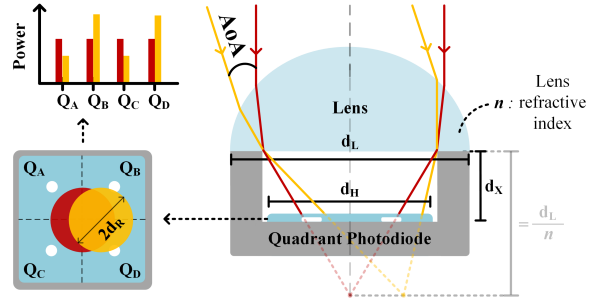


Fig. 3. Diagram of the AoA-sensing VLC RX, i.e., QRX. The red and yellow colors represent conditions for zero and non-zero AoA, respectively.

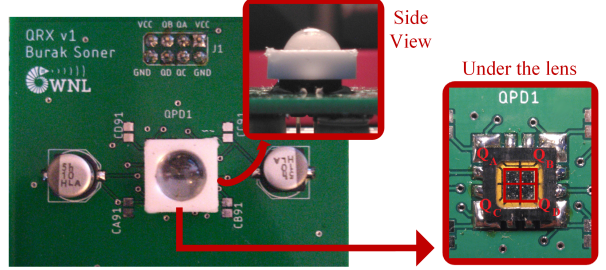


Fig. 4. Picture of the QRX prototype.

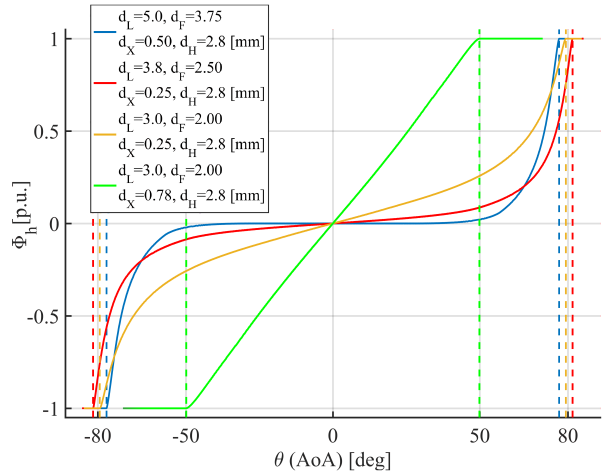


Fig. 5. f_{QRX} for different configurations. Yellow curve provides the best compromise for the design goals: bijection, high FoV and high linearity.

Then, a lens is chosen to set d_L and n such that $2d_R < d_H\sqrt{2}$ is ensured: Since $\{d_L, d_X, d_R, n\} > 0$ in Eqn. (4), d_L upper-limits $2d_R$, thus, setting $d_L < d_H\sqrt{2}$ guarantees bijection alone and makes n a free parameter. Hence, the maximum d_L that satisfies $d_L < d_H\sqrt{2}$ is chosen to also avoid constraining the FoV, and n is chosen solely with regards to low cost.

2) *Choosing the lens-QPD distance:* After setting $\{d_L, n, d_H\}$, d_X is chosen to set $2d_R$ as per Eqn. (4) for the best compromise between FoV and linearity. $d_H < 2d_R$ provides the highest FoV but the mapping is highly non-linear (red curve in Fig. 5). $2d_R \approx d_H$ still results in high FoV ($\approx \pm 80^\circ$) and milder non-linearity (yellow curve in Fig. 5). While $2d_R < d_H$ linearizes the full dynamic range (green curve in Fig. 5), this radically decreases the FoV [43, 53], thus, is not desirable. Therefore, $d_X \approx (d_L - d_H)/n$ is chosen since $2d_R \approx d_H$ provides the best compromise.

IV. PROPOSED VLP-VPE SOLUTION

This section first presents the proposed VLP-based vehicle pose estimation algorithm (VLP-VPE), which uses the QRX design in Section III, and promises restriction-free, cm-level accuracy and >50 Hz rate pose estimation for collision avoidance and platooning, and then derives the performance bound of the algorithm via differential sensitivity analysis [54].

A. Algorithm Description

The algorithm runs on the ego vehicle and computes the relative pose of the target vehicle by a three-step process. First, the AoAs of one TX beam from the target vehicle to two QRXs on the ego vehicle are calculated. Second, using the inter-QRX distance and AoAs from two QRXs, the relative position of the TX unit is computed via triangulation. This constitutes the VLP part. Finally, the same process is repeated for the other TX unit on the same face of the target vehicle. These two positions define the position and orientation of the target vehicle, which corresponds to its relative pose, as shown in Fig. 2b. The algorithm steps are depicted in Fig. 6.

1) Finding the AoA: First, the quadrant readings are sampled at the Nyquist rate of the VLC waveform, $1/T_s$, where T_s is the sampling period, then a number of h_{buf} samples are buffered, and the signal power on each quadrant, ϵ_i , $i \in \{A, B, C, D\}$, is computed by

$$\epsilon_i = \frac{1}{h_{buf}} \left(\sum_{w=w_0}^{w_0+h_{buf}-1} (Q_i[w] - \mu_Q)(s[w]) \right), \quad (5)$$

where w_0 marks the sample time at the beginning of the buffer, $Q_i[w]$ is the reading sample in quadrant i at time wT_s , μ_Q is the constant bias applied to the readings by AC-coupled QRX amplifiers, i.e., $(Q_i[w] - \mu_Q)$ is zero-mean, and $s[w]$ is the received waveform sample at time wT_s , as decoded by the QRX VLC subsystem. w_0 is incremented by h_{buf} for consecutive estimation cycles. This causes the estimation rate to be determined by h_{buf} , i.e., rate = $1/(T_s \times h_{buf})$, and also causes a fixed delay of $(T_s \times h_{buf})/2$ since each estimation cycle produces an average result for a preceding time interval of $(T_s \times h_{buf})$. However, this delay can be ignored since, for the targeted ≥ 50 Hz estimation rate, the delay is ≤ 10 ms, which is negligible considering that even the fastest vehicle transients are ≈ 50 ms because of high inertia [55].

After computing ϵ_i , Φ_h is computed by using Eqn. (3) and the AoA of the TX beam to the QRX is computed by

$$\theta = f_{QRX}^{-1}(\Phi_h) = g_{QRX}(\Phi_h). \quad (6)$$

Eqns. (5) and (6) repeated for both QRXs facing the subject TX yields θ_R and θ_L , which correspond to the AoA calculated at the right and left QRX with their direction determined with respect to the forward-facing frame on the ego vehicle, respectively.

2) Finding the Target TX Unit Positions: Using θ_R , θ_L and the inter-QRX distance, i.e., head/tail light separation, on the ego vehicle, the ${}^e x_{tx}$ and ${}^e y_{tx}$ coordinates of the TX unit on the target vehicle are obtained by

$$k_{tx} = \begin{bmatrix} {}^e x_{tx} \\ {}^e y_{tx} \end{bmatrix} = \begin{bmatrix} d \left(\frac{1}{2} + \frac{\sin(\theta_R) \times \cos(\theta_L)}{\sin(\theta_L - \theta_R)} \right) \\ d \left(\frac{\cos(\theta_R) \times \cos(\theta_L)}{\sin(\theta_L - \theta_R)} \right) \end{bmatrix}, \quad (7)$$

where d is the inter-QRX distance and $k_{tx} = ({}^e x_{tx}, {}^e y_{tx})$ denotes the position of the target TX unit in the ego frame. Eqn. (7) applies to both TX1 and TX2, generating $k_{tx1} = ({}^e x_{tx1}, {}^e y_{tx1})$ and $k_{tx2} = ({}^e x_{tx2}, {}^e y_{tx2})$, respectively.

3) Finding the Target Vehicle Pose: After finding the relative position of one target vehicle TX unit, the calculation is repeated for the other TX unit that faces the ego vehicle QRXs. These two positions, i.e., $k_{tx1} = ({}^e x_{tx1}, {}^e y_{tx1})$ and $k_{tx2} = ({}^e x_{tx2}, {}^e y_{tx2})$, determine the relative pose of the target vehicle as per Eqns. (1) and (2).

B. Performance Analysis

The performance of the proposed algorithm is analyzed and an accuracy bound is obtained via differential sensitivity analysis [54]. Differential sensitivity analysis uses the first partial derivatives of a system transfer function $Y(X_1, X_2, \dots, X_N)$, with respect to its inputs X_j for $j \in \{1, 2, \dots, N\}$, where N is the number of inputs, to obtain a first-order Taylor series approximation of the uncertainty propagation through that system by

$$V(Y) = \sum_{j=1}^N \left(\frac{\delta Y(X_1, X_2, \dots, X_N)}{\delta X_j} \right)^2 V(X_j), \quad (8)$$

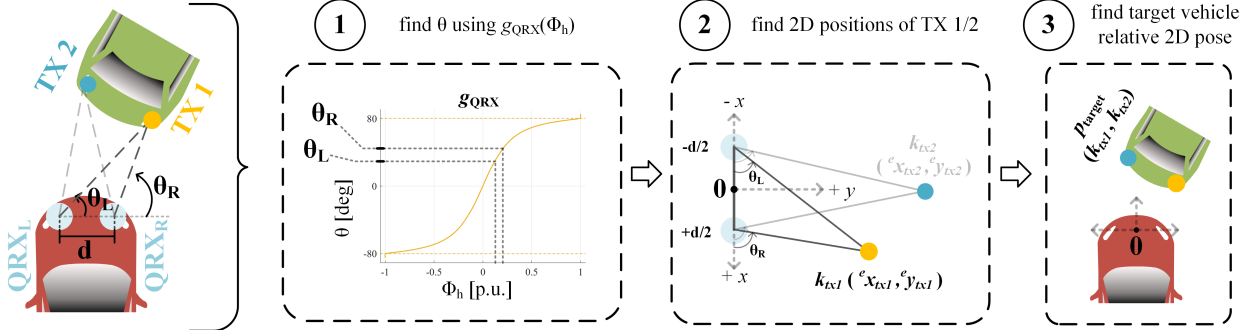


Fig. 6. Algorithm steps of the proposed VLP-VPE solution. The method finds relative pose of the target vehicle in the ego vehicle reference frame.

where $V(Y)$ represents the variance of $Y(X_1, X_2, \dots, X_N)$. The only input of our algorithm is the measured value of $Q_i[w]$ for $i \in \{A, B, C, D\}$, which is only affected by VLC channel noise since there are no systematic errors in the constants and parameters in the system model, i.e., transmitted waveform $s[w]$ is known since reliable communication is sustained (A2) and d , f_{QRX} and μ_Q are measured to sufficient precision *a priori* (A4). Below, we propagate the noise on the estimator input, i.e., $Q_i[w]$, $i \in \{A, B, C, D\}$, to the estimator output, i.e., $k_{tx} = ({}^e x_{tx}, {}^e y_{tx})$, by applying Eqn. (8) to Eqns. (5)-(7) in aggregate fashion, to obtain the performance bound.

The initial step is Eqn. (5), where the powers of the quadrant signals, ϵ_i , are calculated by using the quadrant readings, $Q_i[w]$ for $i \in \{A, B, C, D\}$.

$$V(\epsilon_i) = \sum_{w=w_0}^{w_0+h_{buf}-1} \left(\frac{\delta \epsilon_i}{\delta Q_i[w]} \right)^2 V_Q \quad (9)$$

$$\frac{\delta \epsilon_i}{\delta Q_i[w]} = \frac{s[w]}{h_{buf}}, \quad (10)$$

where V_Q represents $V(Q_i[w])$, which is a constant for $i \in \{A, B, C, D\}$ since the QRXs are well-calibrated, thus, the AWGN on all quadrants have the same power (A4).

Next step is Eqn. (6), where the AoA (θ) is computed using the powers of the quadrant signals, i.e., ϵ_i , $i \in \{A, B, C, D\}$. The following is repeated for both θ_R and θ_L :

$$V(\theta) = \sum_{i=A,B,C,D} \left(\frac{\delta \theta}{\delta \epsilon_i} \right)^2 V(\epsilon_i) \quad (11)$$

$$\frac{\delta \theta}{\delta \epsilon_i} = \left(g'_{QRX}(\Phi_h) \right) \left(\frac{\delta \Phi_h}{\delta \epsilon_i} \right) \quad (12)$$

$$\frac{\delta \Phi_h}{\delta \epsilon_i} = \begin{cases} \frac{-2(\epsilon_B + \epsilon_D)}{(\epsilon_A + \epsilon_B + \epsilon_C + \epsilon_D)^2}, & i = A, C \\ \frac{2(\epsilon_A + \epsilon_C)}{(\epsilon_A + \epsilon_B + \epsilon_C + \epsilon_D)^2}, & i = B, D \end{cases}, \quad (13)$$

where the derivative of g_{QRX} , denoted by g'_{QRX} , is computed numerically since g_{QRX} is saved in the form of a look-up table, as stated in Section III.

The final step considers Eqn. (7) for computing the TX unit positions (k_{tx1} and k_{tx2}) from θ_R and θ_L for each QRX; these two positions define the pose of the target vehicle.

$$V({}^e x_{tx}) = \sum_{m=L,R} \left(\frac{\delta {}^e x_{tx}}{\delta \theta_m} \right)^2 V(\theta_m) \quad (14)$$

$$\frac{\delta {}^e x_{tx}}{\delta \theta_L} = \frac{-d \times \sin(2\theta_R)}{2 \sin^2(\theta_L - \theta_R)}, \quad \frac{\delta {}^e x_{tx}}{\delta \theta_R} = \frac{d \times \sin(2\theta_L)}{2 \sin^2(\theta_L - \theta_R)} \quad (15)$$

$$V({}^e y_{tx}) = \sum_{m=L,R} \left(\frac{\delta {}^e y_{tx}}{\delta \theta_m} \right)^2 V(\theta_m) \quad (16)$$

$$\frac{\delta {}^e y_{tx}}{\delta \theta_L} = \frac{-d \times \cos^2(\theta_R)}{\sin^2(\theta_L - \theta_R)}, \quad \frac{\delta {}^e y_{tx}}{\delta \theta_R} = \frac{d \times \cos^2(\theta_L)}{\sin^2(\theta_L - \theta_R)}. \quad (17)$$

$V({}^e x_{tx})$ and $V({}^e y_{tx})$ denote the final output variance of the estimator, i.e., variances of the distributions of target TX unit x and y coordinate estimations, respectively. Since input noise is AWGN and differential sensitivity analysis considers a linear approximation of the system, the x and y distributions are independent, white and Gaussian. Thus, 99.7% of x and y estimation samples will be bound to three standard deviations, i.e., to intervals of $3 \times \sqrt{V({}^e x_{tx})}$ and $3 \times \sqrt{V({}^e y_{tx})}$ around their respective true values [56]; this constitutes the bound for estimation accuracy.

As a result of this analysis, we observe a trade-off between estimation rate and accuracy against noise, as shown in the following. Substituting Eqn. (10) in Eqn. (9), and moving the constant terms, i.e., h_{buf} and V_Q , out of the summation in Eqn. (9), we obtain

$$V(\epsilon_i) = \frac{V_Q}{h_{buf}^2} \sum_{w=w_0}^{w_0+h_{buf}-1} (s[w])^2 = \frac{\zeta_{h_{buf}}}{h_{buf}^2} V_Q, \quad (18)$$

where $\zeta_{h_{buf}}$ is defined as the energy of $s[w]$ for the h_{buf} interval. Since $\zeta_{h_{buf}}$ is proportional to h_{buf} , let us rewrite $\zeta_{h_{buf}}$ as $\alpha(h_{buf})$, where $\alpha \in \mathbb{R}$ represents the part of $\zeta_{h_{buf}}$ that is independent of h_{buf} . In this case, the h_{buf} terms in Eqn. (18) simplify, and the remaining term, $\alpha V_Q/h_{buf}$, which is constant over the summation indices in Eqns. (11) and (14), can be moved out of the summations as

$$V({}^e x_{tx}) = \frac{\alpha V_Q}{h_{buf}} \sum_{m=L,R} \left(\frac{\delta {}^e x_{tx}}{\delta \theta_m} \right)^2 \sum_{i=A,B,C,D} \left(\frac{\delta \theta}{\delta \epsilon_i} \right)^2. \quad (19)$$

The same steps hold for $V({}^e y_{tx})$. In conclusion, Eqn. (19) shows the trade-off between estimation accuracy and rate: For a given noise level, i.e., given V_Q , estimation accuracy can be improved, i.e., $V({}^e x_{tx})$ and $V({}^e y_{tx})$ can be decreased, by increasing h_{buf} , at the cost of a decrease in the estimation rate, which is equal to $1/(T_s \times h_{buf})$.

V. SIMULATIONS

The simulations demonstrate the performance of the proposed VLP-VPE solution under realistic road and VLC channel conditions in typical collision avoidance and platooning scenarios. A custom MATLAB®-based vehicular VLC simulator was built for this purpose. The simulator utilizes ego and target vehicle trajectories that are either manually generated, or generated from the well-known microscopic traffic simulator SUMO [46], and generates the signals that emanate from the two target TXs and reach the two ego QRXs, for the whole trajectory. The proposed VLP-VPE algorithm then provides relative target pose estimation using these signals. The simulator is available on GitHub [57].

Simulator setup parameters are given in Table I. The QRX design parameters correspond to COTS components for the “best compromise” configuration, i.e., the yellow curve f_{QRX} in Fig. 5. The selected VLC modulation scheme and rate complies with vehicle safety application requirements [32, 58].

TABLE I
SIMULATOR PARAMETERS

VLC TX	Modulation	Binary frequency shift keying
	Carriers	5/7.5 kHz (TX1), 10/12.5 kHz (TX2)
	Data Rate	5 kbps
	Power	1000 lumens (typical tail light)
VLC QRX	DC Bias (μ_Q)	2.5 V
	ADC	Range: [0, 5] V, 16-bit, 100 kSPS
	Lens	PMMA (n=1.5), $d_L = 3$ mm
	QPD	$d_H = 2.8$ mm [59], $d_X = 0.25$ mm
	Amplifier	10000 V _{pk-pk} /lumen, $Z_{out} = 50 \Omega$
	FoV	$\pm 50^\circ$ linear, $\pm 80^\circ$ total (Fig. 5)
Vehicle	Length	5 m
	QRX Separation	1.6 m
	Steering	Ackermann [60] (no side-slipping)

The AWGN is applied directly on $Q_i[w]$ (A4) to include the compound effect of all noise sources. In all simulations, the target vehicle leads the ego vehicle, and thus, the target vehicle transmits through its tail light (similar to Fig. 1). While the opposite configuration is equally valid, this configuration was chosen since it is the worst case scenario; the tail light has the lowest TX power among the vehicle light sources.

We present four simulation scenarios to demonstrate that the proposed solution is eligible for collision avoidance and platooning applications under realistic road and channel conditions:

- *SM1* - localization performance comparison with state-of-the-art. We manually generate the ego and target vehicle trajectories described in [27], simulate our VLP method at the same estimation rate and noise conditions, and show that our method provides higher localization accuracy under fair comparison, advancing the state-of-the-art.
- *SM2* - pose estimation in a collision avoidance scenario. A target vehicle leading an ego vehicle on a highway brakes dangerously during a lane change and risks collision. This scenario relies on manually generated trajectories and demonstrates the performance of the proposed pose estimation solution in a typical pre-crash situation. Results at two different estimation rates are shown to demonstrate the rate-accuracy trade-off identified in the performance analysis. Additionally, the analytical performance bounds for the two estimation rates are also shown together with the simulation results for comparison, and the validity of the bound is discussed.
- *SM3* - pose estimation in a platooning scenario with SUMO. Two vehicles drive back-to-back on a road that is notorious for accidents near Koc University, Istanbul, Turkey; the scenario is simulated in SUMO, as shown in Fig. 7. This scenario demonstrates pose estimation performance for different channel conditions and estimation rates in three ego/target configurations: platooning 1) at close range, i.e., ≤ 10 m, 2) on a road section with extreme ($> 80^\circ$) curvature, and 3) at conventional braking distance, i.e. > 10 m.

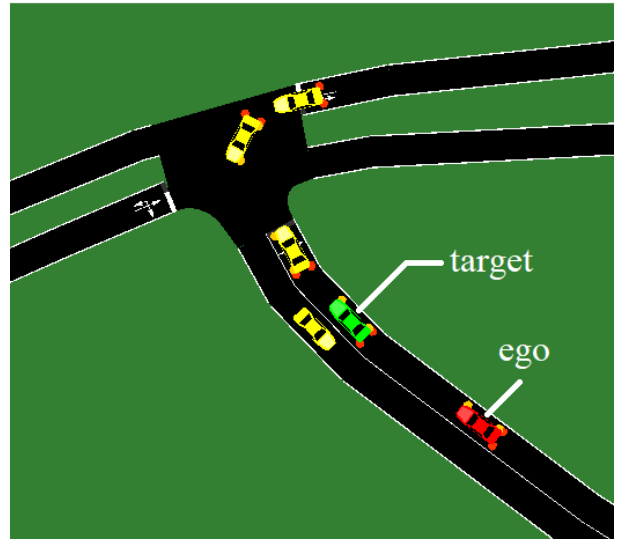


Fig. 7. *SM3* - SUMO screenshot for the road near Koc University.

- *SM4* - effect of inter-vehicular distance on pose estimation accuracy. This scenario exhaustively simulates all feasible target vehicle positions within ego vehicle FoV under different channel conditions, showing the effect of inter-vehicular distance over the complete feasible operational range of the proposed method.

For clarity, we represent the estimation results in these simulations with the midpoint of the two estimated TX positions on the 2D grid.

1) *SM1 - Localization, Comparison with State-of-the-art*: Fig. 8a demonstrates the performance of the proposed method for the ego and target trajectories described in [27], on the 2D grid. To allow fair comparison, the estimation rate of 2 kHz and the noise conditions are the same as in [27]. Fig. 8b shows the x and y coordinate estimation performances of the proposed method separately, whereas Fig. 8c shows the distributions of estimation error for both x and y. While [27] provides higher estimation accuracy in the longitudinal axis, i.e., 6.2 cm error in [27] versus 9.60 cm error in ours, our solution provides superior accuracy in the lateral axis, i.e., 11.3 cm error in [27] versus 2.56 cm error in ours. In terms of overall 2D accuracy, i.e., Euclidean distance from the true position, our solution provides better performance, i.e., 12.9 cm error in [27] versus 9.9 cm error in ours. These results show that our proposed method advances the state-of-the-art for VLP with cm-level localization accuracy and kHz rate under realistic road and channel conditions. Furthermore, the proposed method does not impose any high-bandwidth circuit requirements like [27] and can be extended to pose estimation; the VLP in [27] cannot be extended to pose estimation since it requires parallel target and ego vehicles, as in this scenario.

2) *SM2 - Pose Estimation, Collision Avoidance Scenario*: Fig. 9a shows the actual and estimated trajectories in the *SM2* collision avoidance scenario together with the performance bound derived by the theoretical analysis, for 250 Hz and 1 kHz estimation rates. The AWGN power on the QRXs is -40 dBm in this scenario to better demonstrate the rate-accuracy

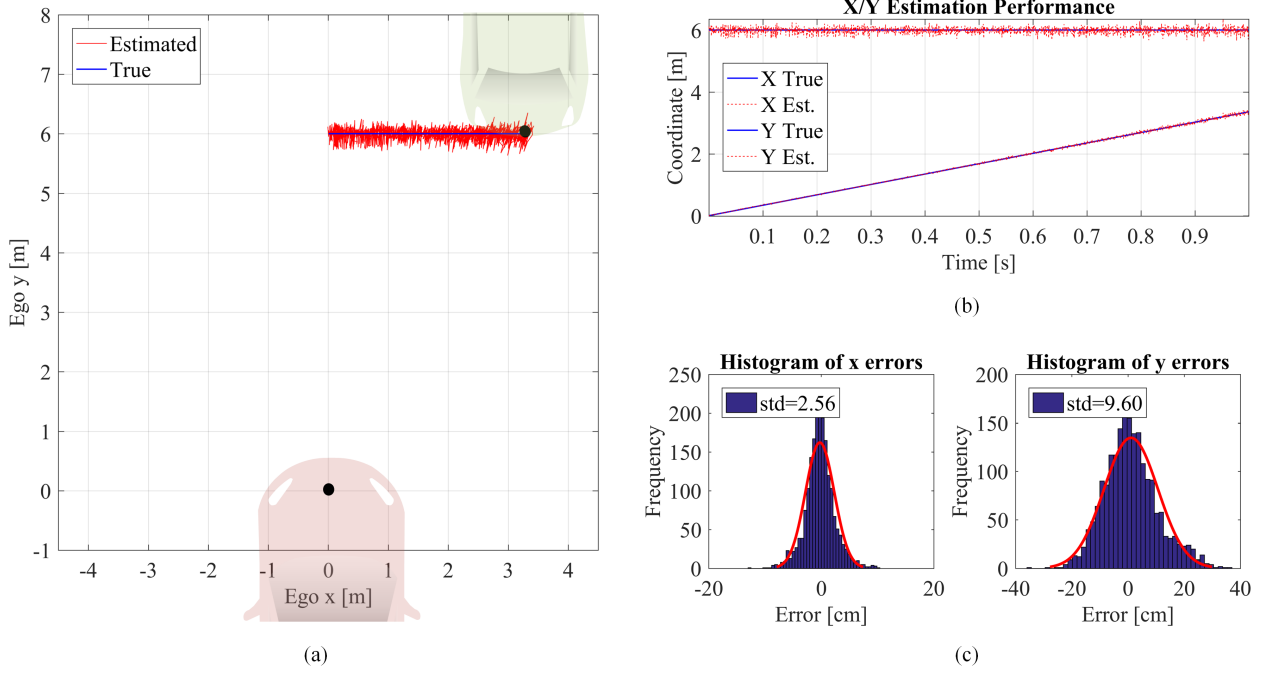


Fig. 8. *SM1 - VLP* results for the trajectory described in [27] at 2 kHz rate, under the same noise conditions as [27]. (a) Localization performance on the 2D grid, (b) x/y individual estimation performances, and (c) histograms of x/y errors with a Gaussian fit.

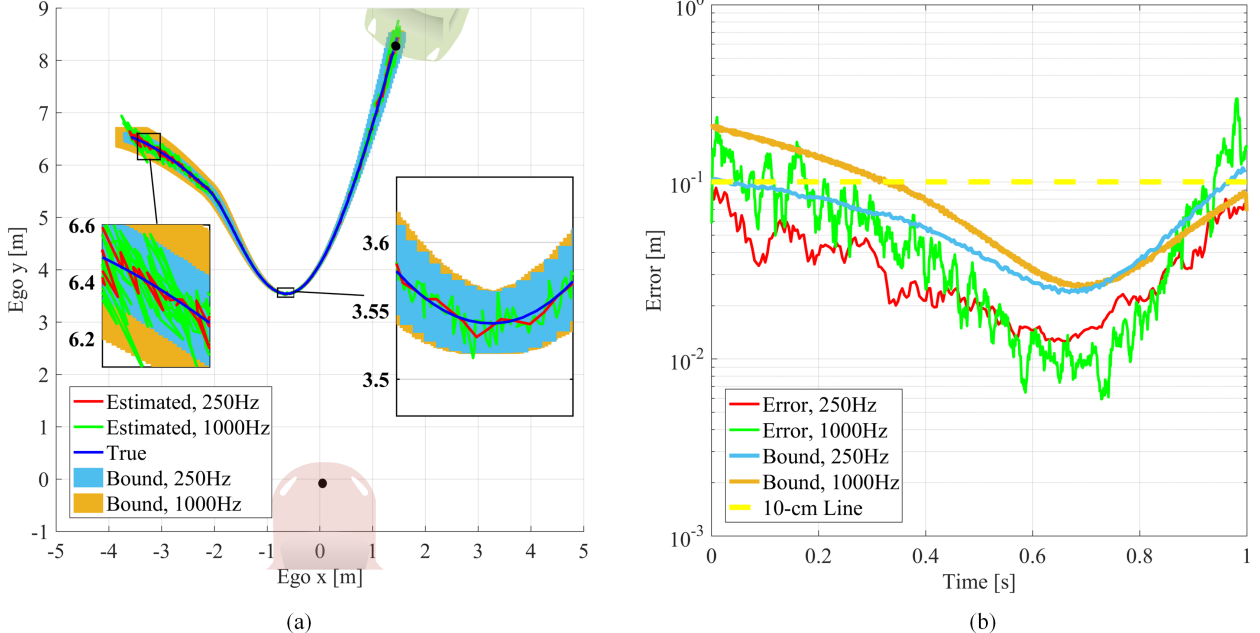


Fig. 9. *SM2 - Pose estimation results for the collision avoidance scenario. (a) Simulation results and theoretical bounds on the 2D grid for 1 kHz and 250 Hz rate under -45 dBm noise, and (b) errors and theoretical bounds for the two runs.*

trade-off. -40 dBm corresponds to very harsh conditions since it is extremely high even for low-end COTS devices. Typical harsh noise figures for low-end devices are \approx -50 dBm.

Fig. 9b verifies the rate-accuracy trade-off identified by the theoretical analysis by showing that the lower estimation rate provides higher overall pose estimation accuracy. While the theoretical bound follows the dynamics of the proposed method correctly, it fails to predict the exact error level in the simulation results over the whole trajectory. This is expected since the analysis uses a local linear approximation of the proposed method, which is globally non-linear. In summary,

the results in this simulation show that the proposed method can provide cm-level, kHz rate pose estimation in pre-crash situations and estimation rate can be sacrificed for higher accuracy under harsh channel conditions.

3) SM3 - Pose Estimation, Platooning Scenario in SUMO: Fig. 10a shows the performance of the proposed method for the SUMO-generated *SM3* trajectory (Fig. 7) on the 2D grid. The scenarios consider both harsh and favorable VLC channel conditions, i.e., -50 dBm and -70 dBm noise power, and estimation rates of 50 Hz and 500 Hz. The errors for each scenario is shown Fig. 10b. In Part I, the vehicles start from rest and

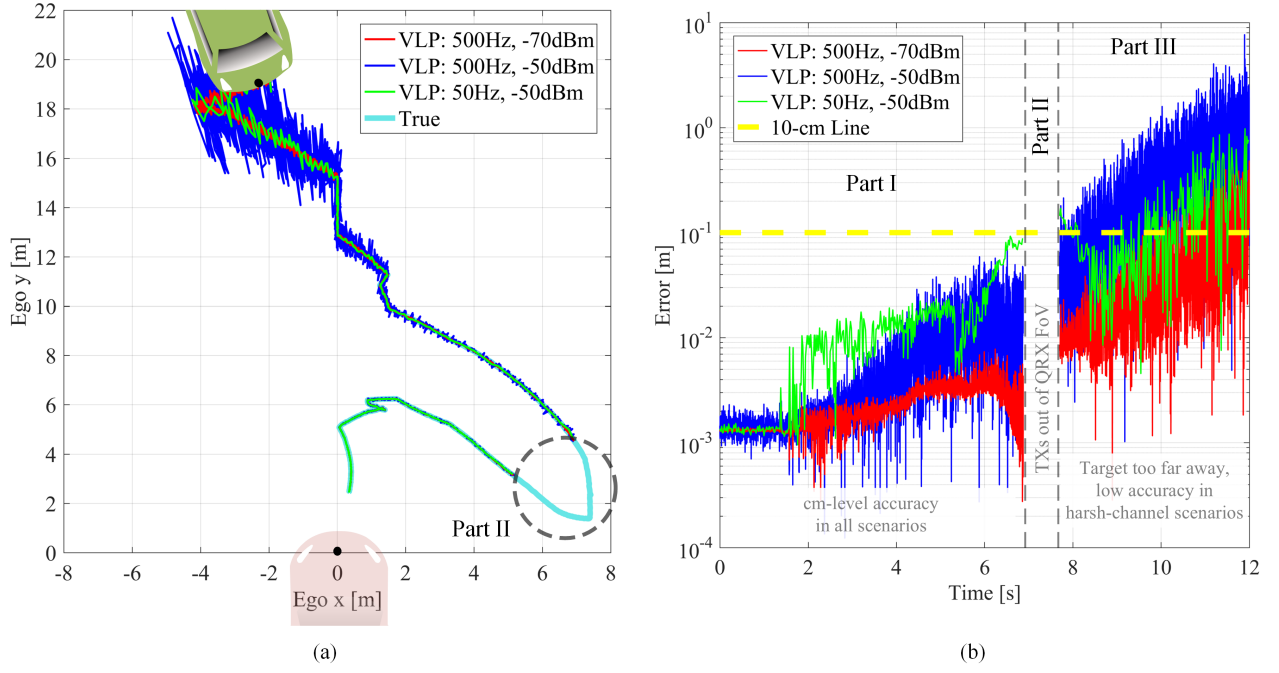


Fig. 10. SM3 - Pose estimation results for the SUMO platooning simulation depicted in Fig. 7. (a) Results for harsh and favorable channel conditions (-70 dBm and -50 dBm noise power, respectively) at different estimation rates (500 Hz and 50 Hz) on the 2D grid. (b) Errors for the same three runs.

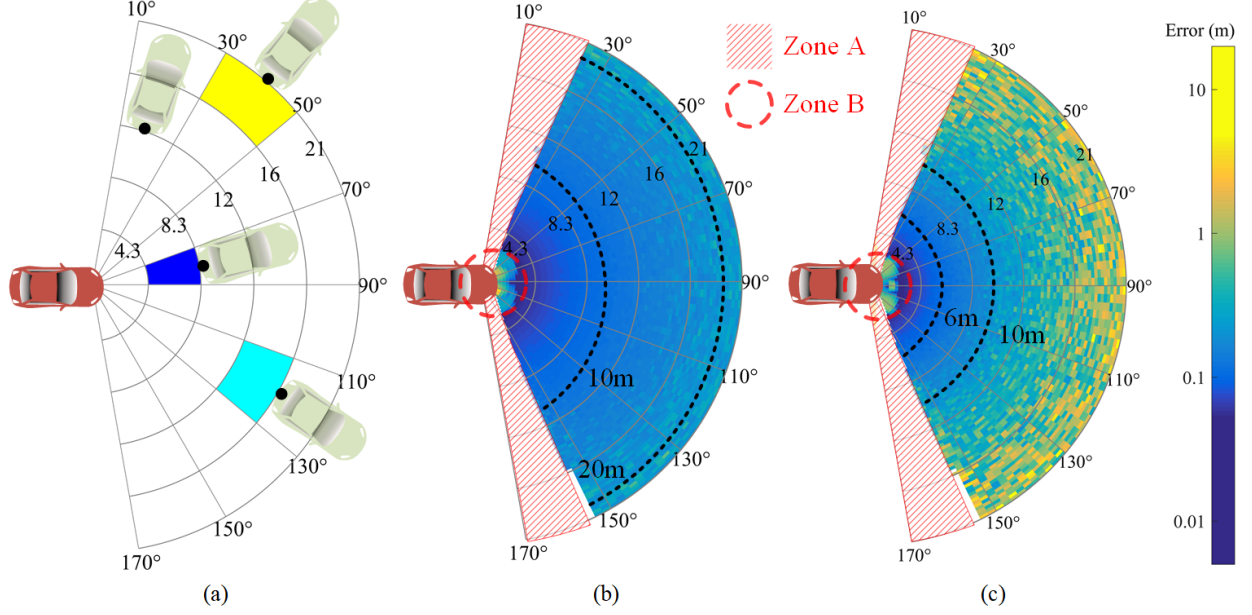


Fig. 11. SM4 - Pose estimation accuracy over the complete feasible operational range at 500 Hz rate. (a) Simulation procedure with representative colors (not estimation results). Results under (b) favorable conditions and (c) harsh conditions.

then move forward into a platoon formation at close range, i.e., ≤ 10 m; all scenarios provide cm-level accuracy in this part but accuracy deteriorates due to the decrease in signal-to-noise ratio as the distance between vehicles increases. In Part II, the target takes the right turn at the intersection shown in Fig. 7 and momentarily breaks the platoon; as expected, the proposed method cannot estimate pose in this region since the LoS link between the TX and QRX is lost, violating assumption A2. In Part III, the LoS is regained and the two vehicles drive back-to-back at conventional braking distance, i.e., >10 m; while cm-level accuracy is lost after >15 m distance only under harsh conditions in this part, platooning at such large distances is not

desirable since it allows high-air-drag “wake zones” to form between vehicles [47]. Due to the rate-accuracy trade-off, the low-rate scenario (green) provides higher accuracy than the high-rate scenario (blue) under harsh conditions. These results show that for feasible platooning configurations, the proposed solution provides cm-level performance at 500 Hz rate under both harsh and favorable conditions, thus, is eligible for use in safe platooning.

4) SM4 - Pose Estimation, The Effect of Target Distance: Fig. 11a shows the procedure in this simulation: Estimation accuracy for sampled target vehicle positions over a 20 m radius, $\pm 80^\circ$ polar grid are evaluated to characterize the feasible

operational range of the proposed solution. The estimation rate is 500 Hz. Figs. 11b and 11c demonstrate pose estimation accuracy under favorable and harsh conditions, respectively, and identify two undesirable zones, i.e. Zones A and B in Fig. 11. In Zone A, target TXs move out of the FoV of ego QRXs; the proposed solution cannot estimate pose in this zone. This effect is also observed in *SM3, Part II*. In Zone B, the target vehicle is too close to the ego vehicle bumper, which means that the TXs are too close to the FoV boundaries of the QRXs; the proposed solution cannot provide cm-level accuracy in this zone. However, these zones are not strictly relevant for collision avoidance and platooning scenarios: Since these scenarios consider ≥ 30 km/h speeds [3], a vehicle in Zone A is at an angle too oblique to be considered as either a platoon element [47] or a tangible collision threat [2], and collision avoidance and safe platooning efforts are futile for Zone B, where the vehicles are too close and collision is almost inevitable. For the remaining regions on the polar grid, the proposed solution promises high accuracy, varying with respect to inter-vehicular distance.

Fig. 11b shows that for favorable channel conditions, i.e., -70 dBm noise power, the promised cm-level accuracy is attained within a ≈ 10 m radius. Up until the ≈ 20 m mark, < 1 m accuracy is attained. On the other hand, under harsh channel conditions, i.e., -50 dBm noise power, cm-level accuracy is limited to a radius of approximately 6 m, as shown in Fig. 11c. The accuracy is still < 1 m up to the 10 m mark, and then degrades to $\approx 1\text{-}10$ m up until the 20 m mark. If necessary, accuracy under harsh conditions can be improved by sacrificing estimation rate, as discussed previously in *SM2* and *SM3*. These results characterize the feasible operational range of the proposed solution and demonstrate that it provides cm-level accuracy at approximately kHz rate even under harsh channel conditions for inter-vehicular distances relevant to collision avoidance and safe platooning applications.

VI. CONCLUSION

This paper proposes a novel VLP-based vehicle pose estimation (VLP-VPE) solution based on the design of a novel low-cost/size VLC receiver (QRX) that can simultaneously provide high-rate communication, and high-accuracy, high-resolution and high-rate AoA measurement. The QRX can be realized with COTS components only, enabling the first practical realization of a vehicle pose estimation solution with cm-level accuracy and kHz rate without imposing any restrictive requirements such as high-bandwidth circuit, localized base station, and VLC waveform constraints, and limited vehicle orientations. The VLP-VPE algorithm uses two QRXs to locate two target vehicle VLC TX units relative to the ego vehicle via VLP, which is sufficient for relative pose estimation. The computational overhead of the solution is very low compared to the conventional LIDAR and camera sensor solutions, which need to scan, locate and process millions of unlabelled points; the proposed solution only needs to locate two labelled points on the target vehicle. Performance of the proposed solution is evaluated with differential sensitivity

analysis and exhaustive simulations on a custom vehicular VLC simulator coupled with the microscopic traffic simulator SUMO. Simulations demonstrate that the proposed solution performs pose estimation with cm-level accuracy at kHz rate even under harsh road and VLC channel conditions. The solution is expected to complement the existing autonomous vehicle sensor system for higher safety by providing pose estimation for collision avoidance and platooning applications.

REFERENCES

- [1] Ford Motor Company, "A matter of trust: Ford's approach to developing self-driving vehicles," 16 Aug 2018. Press Release.
- [2] Statistisches Bundesamt (DESTATIS), "Verkehrsunfälle 2017." https://www.destatis.de/GPStatistik/receive/DEHeft_heft_00083585. Accessed: 2020-03-06.
- [3] K. D. Kusano and H. C. Gabler, "Safety benefits of forward collision warning, brake assist, and autonomous braking systems in rear-end collisions," *IEEE Trans. Intell. Transp. Syst.*, vol. 13, no. 4, pp. 1546–1555, 2012.
- [4] D. Caveney, "Cooperative vehicular safety applications," *IEEE Control Syst. Mag.*, vol. 30, no. 4, pp. 38–53, 2010.
- [5] S. E. Shladover and S.-K. Tan, "Analysis of vehicle positioning accuracy requirements for communication-based cooperative collision warning," *Journal of Intelligent Transportation Systems*, vol. 10, no. 3, pp. 131–140, 2006.
- [6] F. de Ponte Müller, "Survey on ranging sensors and cooperative techniques for relative positioning of vehicles," *Sensors*, vol. 17, no. 2, p. 271, 2017.
- [7] Y. Feng, J. Wang, et al., "GPS RTK performance characteristics and analysis," *Positioning*, vol. 1, no. 13, 2008.
- [8] A. Mukhtar, L. Xia, and T. B. Tang, "Vehicle detection techniques for collision avoidance systems: A review," *IEEE Trans. Intell. Transp. Syst.*, vol. 16, no. 5, pp. 2318–2338, 2015.
- [9] H. Badino, U. Franke, and D. Pfeiffer, "The stixel world - A compact medium level representation of the 3D world," in *Joint Pattern Recognition Symposium*, pp. 51–60, Springer, 2009.
- [10] M. J. Leotta and J. L. Mundy, "Vehicle surveillance with a generic, adaptive, 3D vehicle model," *IEEE Trans. Pattern Anal. Mach. Intell.*, vol. 33, no. 7, pp. 1457–1469, 2010.
- [11] H. Lategahn and C. Stiller, "Vision-only localization," *IEEE Trans. Intell. Transp. Syst.*, vol. 15, no. 3, pp. 1246–1257, 2014.
- [12] K. Abboud, H. A. Omar, and W. Zhuang, "Interworking of DSRC and cellular network technologies for V2X communications: A survey," *IEEE Trans. Veh. Technol.*, vol. 65, no. 12, pp. 9457–9470, 2016.
- [13] L. N. Balico, A. A. Loureiro, E. F. Nakamura, R. S. Barreto, R. W. Pazzi, and H. A. Oliveira, "Localization prediction in vehicular ad hoc networks," *IEEE Commun. Surveys Tuts.*, vol. 20, no. 4, pp. 2784–2803, 2018.
- [14] S.-H. Yu, O. Shih, H.-M. Tsai, N. Wisitpongphan, and R. D. Roberts, "Smart automotive lighting for vehicle safety," *IEEE Commun. Mag.*, vol. 51, no. 12, pp. 50–59, 2013.
- [15] G. Gurbilek, M. Koca, A. Uyurus, B. Soner, E. Basar, and S. Coleri, "Location-aware adaptive physical layer design for vehicular visible light communication," in *2019 IEEE Vehicular Networking Conference (VNC)*, pp. 1–4, IEEE, 2019.
- [16] H. Liu, H. Darabi, P. Banerjee, and J. Liu, "Survey of wireless indoor positioning techniques and systems," *IEEE Trans. Syst., Man, Cybern. Syst., Part C (Applications and Reviews)*, vol. 37, no. 6, pp. 1067–1080, 2007.
- [17] F. Gustafsson and F. Gunnarsson, "Mobile positioning using wireless networks: possibilities and fundamental limitations based on available wireless network measurements," *IEEE Signal Process. Mag.*, vol. 22, no. 4, pp. 41–53, 2005.
- [18] R. Klukas and M. Fattouche, "Line-of-sight angle of arrival estimation in the outdoor multipath environment," *IEEE Trans. Veh. Technol.*, vol. 47, no. 1, pp. 342–351, 1998.
- [19] A. Broumandan, T. Lin, J. Nielsen, and G. Lachapelle, "Practical results of hybrid AoA/TDOA geo-location estimation in CDMA wireless networks," in *2008 IEEE 68th Vehicular Technology Conference*, pp. 1–5, IEEE, 2008.
- [20] J. Chen and A. Abedi, "A hybrid framework for radio localization in broadband wireless systems," in *2010 IEEE Global Telecommunications Conference GLOBECOM 2010*, pp. 1–6, IEEE, 2010.

- [21] M. Ciurana, D. López, and F. Barceló-Arroyo, "SoftOA: Software ranging for TOA-based positioning of WLAN terminals," in *International Symposium on Location-and Context-Awareness*, pp. 207–221, Springer, 2009.
- [22] N. Alam, A. T. Balaei, and A. G. Dempster, "A cooperative positioning method for VANETs using DSRC carrier frequency offset," in *Int. Global Navigation Satellite Systems (IGNSS) Symp.*, Citeseer, 2011.
- [23] N. Alam and A. G. Dempster, "Cooperative positioning for vehicular networks: Facts and future," *IEEE Trans. Intell. Transp. Syst.*, vol. 14, no. 4, pp. 1708–1717, 2013.
- [24] Y. Zhuang, L. Hua, L. Qi, J. Yang, P. Cao, Y. Cao, Y. Wu, J. Thompson, and H. Haas, "A survey of positioning systems using visible LED lights," *IEEE Commun. Surveys Tuts.*, vol. 20, no. 3, pp. 1963–1988, 2018.
- [25] B. Bai, G. Chen, Z. Xu, and Y. Fan, "Visible light positioning based on LED traffic light and photodiode," in *2011 IEEE Vehicular Technology Conference (VTC Fall)*, pp. 1–5, IEEE, 2011.
- [26] R. Roberts, P. Gopalakrishnan, and S. Rathi, "Visible light positioning: Automotive use case," in *2010 IEEE Vehicular Networking Conference*, pp. 309–314, IEEE, 2010.
- [27] B. Béchadergue, L. Chassagne, and H. Guan, "A visible light-based system for automotive relative positioning," in *2017 IEEE SENSORS*, pp. 1–3, IEEE, 2017.
- [28] B. Béchadergue, *Visible light range-finding and communication using the automotive LED lighting*. PhD thesis, Université Paris Saclay, English, 2017.
- [29] M. F. Keskin, A. D. Sezer, and S. Gezici, "Localization via visible light systems," *Proc. IEEE*, vol. 106, no. 6, pp. 1063–1088, 2018.
- [30] T. Yamazato and S. Haruyama, "Image sensor based visible light communication and its application to pose, position, and range estimations," *IEICE transactions on communications*, vol. 97, no. 9, pp. 1759–1765, 2014.
- [31] T. Yamazato, I. Takai, H. Okada, T. Fujii, T. Yendo, S. Arai, M. Andoh, T. Harada, K. Yasutomi, K. Kagawa, et al., "Image-sensor-based visible light communication for automotive applications," *IEEE Commun. Mag.*, vol. 52, no. 7, pp. 88–97, 2014.
- [32] A.-M. Căilean and M. Dimian, "Current challenges for visible light communications usage in vehicle applications: A survey," *IEEE Commun. Surveys Tuts.*, vol. 19, no. 4, pp. 2681–2703, 2017.
- [33] C. He, S. Cincotta, M. M. A. Mohammed, and J. Armstrong, "Angular diversity aperture (ADA) receivers for indoor multiple-input multiple-output (MIMO) visible light communications (VLC)," *IEEE Access*, vol. 7, pp. 145282–145301, 2019.
- [34] B. Zhu, Z. Zhu, Y. Wang, and J. Cheng, "Optimal optical omnidirectional angle-of-arrival estimator with complementary photodiodes," *Journal of Lightwave Technology*, vol. 37, no. 13, pp. 2932–2945, 2019.
- [35] A. Arafa, X. Jin, and R. Klukas, "Wireless indoor optical positioning with a differential photosensor," *IEEE Photon. Technol. Lett.*, vol. 24, no. 12, pp. 1027–1029, 2012.
- [36] S. Lee and S.-Y. Jung, "Location awareness using angle-of-arrival based circular-PD-array for visible light communication," in *2012 18th Asia-Pacific Conference on Communications (APCC)*, pp. 480–485, IEEE, 2012.
- [37] P.-W. Lu and R. Chen, "Infrared-based vehicular positioning with the automatic radiation-strength control," *IET Intelligent Transport Systems*, vol. 8, no. 3, pp. 273–285, 2013.
- [38] T. Q. Wang, R. J. Green, and J. Armstrong, "Prism array-based receiver with application in MIMO indoor optical wireless communications," in *2014 16th International Conference on Transparent Optical Networks (ICTON)*, pp. 1–4, IEEE, 2014.
- [39] E. Aparicio-Esteve, Á. Hernández, J. Ureña, and J. M. Villadangos, "Visible light positioning system based on a quadrant photodiode and encoding techniques," *IEEE Trans. Instrum. Meas.*, 2019.
- [40] S. Cincotta, A. Neild, C. He, and J. Armstrong, "Visible light positioning using an aperture and a quadrant photodiode," in *2017 IEEE Globecom Workshops (GC Wkshps)*, pp. 1–6, IEEE, 2017.
- [41] J. M. Kahn and J. R. Barry, "Wireless infrared communications," *Proc. IEEE*, vol. 85, no. 2, pp. 265–298, 1997.
- [42] T. Q. Wang, Y. A. Sekercioğlu, and J. Armstrong, "Analysis of an optical wireless receiver using a hemispherical lens with application in MIMO visible light communications," *Journal of Lightwave Technology*, vol. 31, no. 11, pp. 1744–1754, 2013.
- [43] R. Carbonneau, J. Dubois, and G. Harris, "An optical gun muzzle sensor to improve firing accuracy," in *Optical Testing and Metrology*, vol. 661, pp. 352–358, International Society for Optics and Photonics, 1986.
- [44] B. Soner and S. C. Ergen, "A Low-SWaP, Low-Cost Transceiver for Physically Secure UAV Communication with Visible Light," in *International Symposium on Innovative and Interdisciplinary Applications of Advanced Technologies*, pp. 355–364, Springer, 2019.
- [45] B. Soner and S. C. Ergen, "Vehicular visible light positioning with a single receiver," in *2019 IEEE 30th Annual International Symposium on Personal, Indoor and Mobile Radio Communications (PIMRC)*, pp. 1–6, IEEE, 2019.
- [46] P. A. Lopez, M. Behrisch, L. Bieker-Walz, J. Erdmann, Y.-P. Flötteröd, R. Hilbrich, L. Lücke, J. Rummel, P. Wagner, and E. WieBner, "Microscopic traffic simulation using sumo," in *2018 21st International Conference on Intelligent Transportation Systems (ITSC)*, pp. 2575–2582, IEEE, 2018.
- [47] P. Jootel, "SAfe road TRains for the environment," *SARTRE Project, Final Project Report*, 2012.
- [48] American Association of Highway and Transportation Officials (AASHTO), "Chapter 3.4.6: Vertical curves," in *A Policy on Geometric Design of Highways and Streets, 7th edition*, pp. 295–310, 2011.
- [49] H. Wu, S. Cheng, Y. Peng, K. Long, and J. Ma, "IEEE 802.11 distributed coordination function (DCF): analysis and enhancement," in *2002 IEEE International Conference on Communications. Conference Proceedings. ICC 2002 (Cat. No. 02CH37333)*, vol. 1, pp. 605–609, IEEE, 2002.
- [50] H. Hartenstein and L. Laberteaux, "A tutorial survey on vehicular ad hoc networks," *IEEE Commun. Mag.*, vol. 46, no. 6, pp. 164–171, 2008.
- [51] Edmund Optics, Edmund Optics Tech Tools, "Focal length calculator." <https://www.edmundoptics.com/resources/tech-tools/focal-length>. Accessed: 2019-10-06.
- [52] L. M. Manojlović, "Quadrant photodetector sensitivity," *Applied optics*, vol. 50, no. 20, pp. 3461–3469, 2011.
- [53] H. Steendam, T. Q. Wang, and J. Armstrong, "Cramer-Rao bound for indoor visible light positioning using an aperture-based angular-diversity receiver," in *2016 IEEE International Conference on Communications (ICC)*, pp. 1–6, IEEE, 2016.
- [54] D. Hamby, "A review of techniques for parameter sensitivity analysis of environmental models," *Environmental monitoring and assessment*, vol. 32, no. 2, pp. 135–154, 1994.
- [55] G. Vandi, D. Moro, F. Ponti, R. Parenti, and G. Einaudi, "Vehicle dynamics modeling for real-time simulation," tech. rep., SAE Technical Paper, 2013.
- [56] M. E. Cunningham, C. R. Hann, and A. R. Olsen, "Uncertainty analysis and thermal stored energy calculations in nuclear fuel rods," *Nuclear Technology*, vol. 47, no. 3, pp. 457–467, 1980.
- [57] Burak Soner, and Sinem Coleri, *Vehicular VLC-VLP-VPE Simulator*. https://github.com/sonebu/v2lc_sim.
- [58] CAMP Vehicle Safety Communications Consortium, "Vehicle safety communications project: Task 3 final report: identify intelligent vehicle safety applications enabled by DSRC," *NHTSA, US Department of Transportation, Washington DC*, 2005.
- [59] TT Electronics, "Datasheet, OPR5911 Quadrant Photodiode."
- [60] J. Ackermann, "Robust decoupling of car steering dynamics with arbitrary mass distribution," in *Proceedings of 1994 American Control Conference-ACC'94*, vol. 2, pp. 1964–1968, IEEE, 1994.